ISSN 0023-1584, Kinetics and Catalysis, 2009, Vol. 50, No. 5, pp. 705–714. © Pleiades Publishing, Ltd., 2009.
Original Russian Text © S.A. Solov'ev, S.N. Orlik, 2009, published in Kinetika i Kataliz, 2009, Vol. 50, No. 5, pp. 734–744.

Structural and Functional Design of Catalytic Converters for Emissions from Internal Combustion Engines

S. A. Solov'ev and S. N. Orlik

Pisarzhevskii Institute of Physical Chemistry, National Academy of Sciences of Ukraine, Kiev, Ukraine
e-mail: soloviev@inphyschem-nas.kiev.ua, orlyk@inphyschem-nas.kiev.ua

Received December 1, 2006; in final form, May 5, 2008

Abstract—We consider some features of technology for manufacturing advanced three-way ($CO/NO_x/C_nH_m$) catalytic converters for emissions of internal combustion engines, namely, application, stabilization, and modification of γ-Al_2O_3 second supports on synthetic cordierite matrices and Pt, Pd, and Rh active components, as well as oxidation of finely divided carbon on the surface of soot filters coated with a catalyst coating in the form of binary oxide compositions ($CuCr_2O_4$ and $CuCo_2O_4$) using a number of oxidizers (O_2, O_3, NO, NO_2, H_2O, and CO_2).

DOI: 10.1134/S0023158409050127

Conversion of emissions from internal combustion engines is a very complex and challenging problem of protecting the environment from toxic pollutants, including both reductants (carbon monoxide and hydrocarbons) and oxidizers (nitrogen oxides).

Severe requirements are imposed on catalytic converters. Therefore, a catalytic converter for the neutralization of emissions of internal combustion engines (a three-way catalytic converter, $CO/NO_x/C_nH_m$, TWC) is a complex system comprising a ceramic or metallic monolith support coated with a second support layer that has a sufficiently large specific surface area (as a rule, second support layers are metastable alumina phases) [1–3]. The most promising support materials are natural or synthetic aluminosilicates (cordierites) [2, 4]. Supported phases can contain CeO_2–ZrO_2 mixtures, whose function is to accumulate oxygen [5, 6]; rare-earth and alkaline-earth metal oxides to stabilize low-temperature alumina phases [7–10]; and platinum-group metals (Pt, Pd, Rh, and Ru) to provide the conversion of the toxic components of emissions to CO_2, N_2, and H_2O [11–13].

Now, minimization of the specific consumption of platinum metals in all their applications is among the main strategies of research and technology. The main line of advances in TWCs is concerned with their modification to decrease precious metal percentages by means of nanotechnologies [14, 15].

Processes for manufacturing exhaust gas converters for gasoline engines are described in a number of relevant surveys [1, 16–18]. Conversion technologies for diesel emissions are much farther from optimization. Inasmuch as diesel fuels contain high-carbon fractions of heavy oils, diesel emissions contain soot (to 65 mg/m^3) produced by incomplete combustion of heavy fractions of crude oils (the main components of diesel fuels). Therefore, one challenge in the use of internal combustion engines, primarily, diesels, is removal of soot particles from emissions; carbon particles do not combust on TWCs containing platinum-group metals. Removal of solid microparticulates is especially challenging in view of the expected introduction of EURO-5 standards in the EC, which impose severe limitations on the soot levels of automobile emissions. The most efficient solution in soot conversion technology is a combination of soot filter and soot oxidizer functions in one unit [19]. Recently, attempts have been made to design catalyst coatings for improving the efficiency of soot filters [20] and oxidizing carbonaceous particles directly in soot filters at exhaust gas temperatures [21, 22]. Investigations into this field follow two major routes, one oriented to improve the efficiency of contact between soot and the catalyst surface [20, 23–27] and the other using NO, NO_2 [28, 29], or SO_2 [30] as soot oxidizers.

Here, we consider some aspects of advanced TWC technology (application, stabilization, and modification of a γ-Al_2O_3 second support and platinum, palladium, and rhodium active components). We also concern the oxidation of finely divided carbon on the surface of soot filters coated with a catalyst coating in the form of binary oxide compositions using a number of oxidizers (O_2, O_3, NO, NO_2, H_2O, and CO_2).

EFFECT OF A γ-Al_2O_3 SECOND SUPPORT ON PHYSICOCHEMICAL PARAMETERS OF THREE-WAY CATALYTIC CONVERTERS

Ceramic monolith matrices of honeycomb structure made of synthetic cordierite ($2Al_2O_3 \cdot 2MgO \cdot 5SiO_2$) designed and manufactured at the Institute of

Table 1. Specific surface areas of ceramic/monolith matrices coated with a second support as a function of calcining temperature

Second support percentage	S_{sp}, m^2/g, after treatment at, °C				
	550	760	900	1000	1200
6.3% Al_2O_3	8.2	4.6	2.1	0.6	0.5
10.2% Al_2O_3	12.2	7.9	4.3	1.0	0.7
14.5% Al_2O_3	16.5	9.1	5.2	1.3	1.0
13.8% Al_2O_3 + 1.3% REO	14.2	12.1	9.3	3.0	3.0
12.8% Al_2O_3 + 2.6% REO	12.0	11.0	9.0	3.0	3.0

Materials Sciences Problems, National Academy of Sciences of Ukraine, with cell sizes of 1.0 × 1.0 mm and wall thickness of 0.2 mm, were used as catalyst supports. Their crush strength was 50 MPa along channels and 20 MPa across channels. γ-Al_2O_3, which combines thermal stability with a developed pore structure was chosen as a second support material [2]. Compositions useful for the formation of second support layers on ceramic matrices in the form of alumina, as a rule, contain aluminum oxynitrates of various structures. Analysis of thermogravimetric and X-ray powder diffraction data and related literature [31, 32] suggests the following scheme for aluminum nitrate decomposition:

$$\mathrm{Al(NO_3)_3 \cdot 9H_2O}\ (120\text{–}140^\circ\mathrm{C}) \longrightarrow \mathrm{Al(NO_3)(OH)_2 \cdot 5H_2O}\ (150\text{–}180^\circ\mathrm{C}) \longrightarrow \mathrm{Al(NO_3)(OH)_2}, \mathrm{Al_2O_3 \cdot 3H_2O}, \mathrm{Al_2O_3 \cdot 2H_2O}, \mathrm{Al_2O_3 \cdot H_2O}\ (200\text{–}250^\circ\mathrm{C}) \longrightarrow \mathrm{Al_2O_3 \cdot H_2O}\ (350\text{–}450^\circ\mathrm{C}) \longrightarrow \text{ultrafine } \gamma\text{-}\mathrm{Al_2O_3}\ (500\text{–}550^\circ\mathrm{C}).$$

Aluminum oxynitrates are formed from $Al(NO_3)_3 \cdot 9H_2O$ within the range 140–180°C. Their general formula can be written as $Al(OH)_l(NO_3)_m \cdot nH_2O$, where $l = 1\text{–}2$, $m = 1\text{–}2$, and $n = 0\text{–}2$. The indices l, m, and n are functions of temperature, synthesis duration, and water vapor pressure in the reaction zone. The aluminum oxynitrate composition providing the formation of a stable colloid solution having the required kinematic viscosity and not breaking for long periods of time has been determined. Solutions having pH of 3.5–4.0 and density of 1.348 g/cm^3 and containing 0.15 g/cm^3 of aluminum salts (calculated as Al_2O_3) were found to be optimal for alumina application. These solutions favor the formation of finely divided alumina on cordierite ceramic matrices [32] and thereby ensure good adhesion of the second support to the smooth surface of the ceramic matrix.

Table 1 lists the BET specific surface areas S_{sp} determined using thermal nitrogen adsorption for ceramic monolith supports containing various Al_2O_3 percentages. The surface area of an initial monolith matrix is 0.42 m^2/g. Doping the second support with rare-earth oxides (REOs) slightly decreases specific surface areas. Special experiments showed that, after a sample was coated with 16.5% γ-Al_2O_3, its porosity determined from water vapor adsorption decreased from 23.0 to 19.5%.

Figure 1 displays micrographs of a fractured ceramic monolith matrix sample containing 14.5% γ-Al_2O_3 as a second support obtained by scanning electron microscopy in tandem with electron probe microanalysis on CAMECA SX-50. This sample is characterized by uniform distributions of two types of porosities: isolated pores 0.5–1.0 μm in size lying inside large grain assemblies (Fig. 1a) or along broken grain boundaries (Fig. 1b); and large channel pores with the ratios of the length to average cross section (form factors) within 3–5 and diameters of about 10 μm, which can function as transport pores in the catalytic converter (Fig. 1a), as described in [1].

Treatment at temperatures above 600°C induces the transition of γ-Al_2O_3 to other polymorphs with lower specific surface areas. Lanthanum, cerium, yttrium, and some rare-earth oxides alter the thermal stability of the pore structure of Al_2O_3 coatings [2, 7], probably because of forming spinel (perovskite) structures, but each rare-earth oxide has its own effect.

The mechanism of the thermostabilizing effects of REOs and other oxides on low-temperature alumina phases has been a point of discussion for several years [1, 7, 9, 33–35]. The efficiency of a dopant is hardly predictable and is dictated by both the dopant concentration and the Al_2O_3 synthesis parameters [1, 9]. Mutual influence of several REOs on the properties of low-temperature alumina phases has not been studied, although the utility of metal oxide mixtures (CeO_2 and ZrO_2) for improving the thermal stability of γ-Al_2O_3 has been considered [1, 7, 16]. Therefore, the thermal stability, pore structure parameters, and adsorption properties of finely divided Al_2O_3 samples prepared by sol–gel technology were studied as affected by REO dopants (CeO_2, La_2O_3, and their mixtures) [36]. The phase composition of these samples was studied by X-ray diffraction on DRON-3M. After heat treatment at 550, 700, and 850°C, the samples are mostly X-ray amorphous. The X-ray diffraction patterns of the samples calcined at 850°C, which coincide with the X-ray diffraction pattern of undoped Al_2O_3, contain only weak broad halos at $2\theta = 28.6^\circ$ and 38.5° and a broad

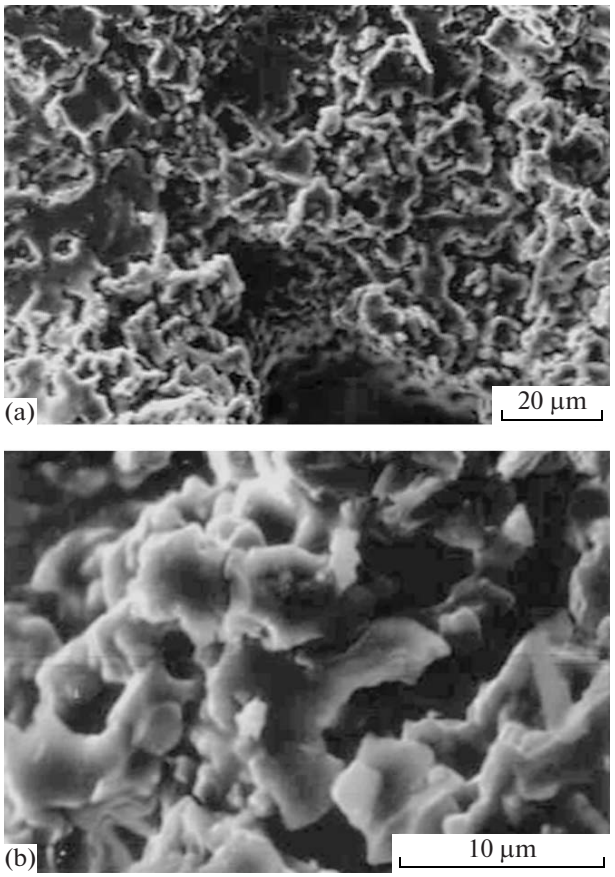

Fig. 1. Electron micrographs of ceramic/monolith matrices coated with γ-Al_2O_3 (14.5%): (a) ×1000 and (b) ×4000.

weak reflection at $2\theta = 65.9°$; these features correspond to the γ-Al_2O_3 structure. Well-defined crystallization of the components of the systems studied occurs at 1000°C (Fig. 2). For example, the X-ray diffraction pattern of a lanthanum-doped sample after calcining at 1000°C (Fig. 2, curve *1*) coincides with the pattern of undoped alumina (850°C) and corresponds to a finely divided γ-Al_2O_3 phase. As the La_2O_3 level increases from 2% (Fig. 2, curve *1*) to 5% (Fig. 2, curve *2*), the characteristic γ-Al_2O_3 reflections are reduced in intensity. For samples doped with mixed REOs (Table 2; samples 5, 6), characteristic CeO_2 reflections ($2\theta = 28.4°$, 32.8°, 47.4°, 56.2°, 76.5°, 78.9°, 88.4°) appear on the background of the Al_2O_3 diffraction pattern, as shown by X-ray diffraction patterns *3* and *4* in Fig. 2. Calcining a CeO_2/Al_2O_3 sample at 1000°C makes a cerium oxide to segregate into an autonomous phase with the transition of part of the γ-Al_2O_3 to corundum α-Al_2O_3 (Fig. 2, curve *5*), as in undoped alumina. This explains while S_{sp} for the cerium-doped sample (Table 2, sample 4) is lower than for the lanthanum-doped sample after heat treatment at 1000°C (Table 2; samples 2, 3).

Inasmuch as there is no intrinsic crystallization of lanthanum oxide and lanthanum aluminates, we should think that the stabilizing effect of REOs is due to the formation of solid solutions of lanthanum in Al_2O_3; these solid solutions are X-ray amorphous and, because of their high dispersion and disorder, do not exist as an autonomous phase below 1000°C in agreement with the results of similar studies [7]. Thus, REOs, in particular, La_2O_3, CeO_2, and their mixtures,

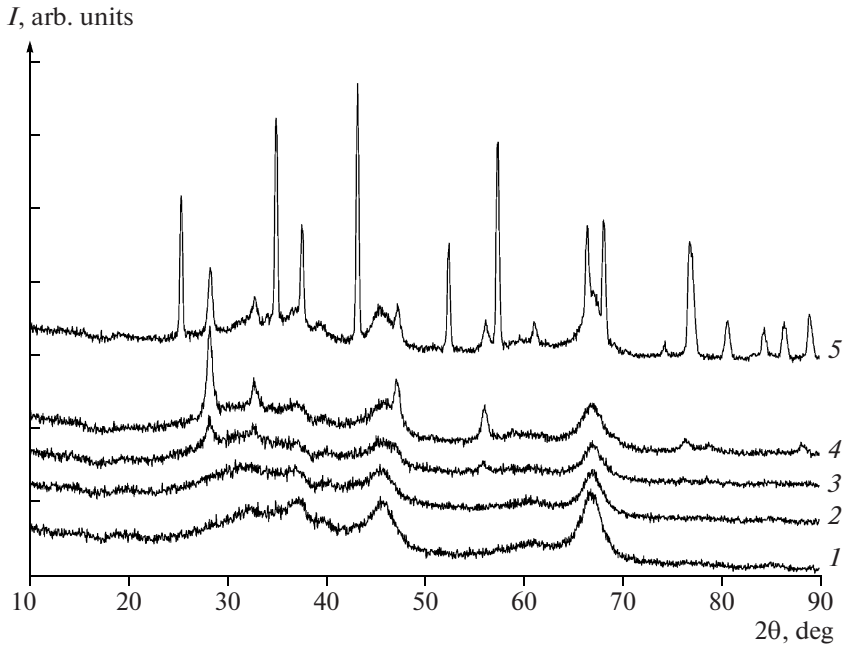

Fig. 2. X-ray diffraction patterns from REO-modified Al_2O_3 samples after treatment at 1000°C: (*1*) Al_2O_3/2% La_2O_3, (*2*) Al_2O_3/5% La_2O_3, (*3*) Al_2O_3/(5% La_2O_3 + 2.5% CeO_2), (*4*) Al_2O_3/(2.5% La_2O_3 + 5% CeO_2), and (*5*) Al_2O_3/5% CeO_2.

Table 2. Effect of dopant REO and calcining temperature on the Al_2O_3 specific surface area

Sample no.	REO percentage, wt %		S_{sp}, m^2/g, after treatment at, °C			
	CeO_2	La_2O_3	550	700	850	1000
1	0	0	176	167	142	10
2	0	2.0	176	153	142	86
3	0	5.0	132	144	112	62
4	5.0	0	166	180	130	20
5	5.0	2.5	124	160	124	69
6	2.5	5.0	142	149	112	56

improve the thermal stability of the pore structure of finely dispersed Al_2O_3. The highest stabilizing effect of La_2O_3 is on account of the formation of a La_2O_3 solid solution in Al_2O_3, which inhibits aluminum ion diffusion and retards the transition of low-temperature Al_2O_3 phases to high-temperature α-Al_2O_3.

The data displayed in Table 1 also imply that the treatment of γ-Al_2O_3-coated ceramic monolith matrices at 900°C induces a three- to fourfold decrease in S_{sp}. The thermal stability of coatings on samples containing REOs modifying dopants [36, 37] is far higher; after heat treatment in the specified mode, the decrease in S_{sp} does not exceed 25–35%. When the treatment temperature is 1000–1200°C, the decrease in S_{sp} is considerable and the effect of REOs is canceled out. Thus, the thermal stability of the pore structure of the coating increases to 900°C as a result of the modification of the alumina second support by REOs with doping levels up to 1.3–2.6 wt %.

Converters based on γ-Al_2O_3-coated honeycomb monolith matrices were prepared as follows: the support was impregnated consecutively with proper metal (Pt, Pd, and Rh) salts, and monoliths were purged with compressed air to remove residual solution, followed by drying in flowing air at 100–120°C and calcining at the temperatures at which salts decompose: 550°C (H_2PtCl_6), 350°C ($Pd(NO_3)_2$), and 450°C ($RhCl_3$).

Catalytic activities were characterized by the CO and *n*-hexane conversion (*X*) in oxidation by atmospheric oxygen for CO = 1.6 vol % and n-C_6H_{14} = 1.1 vol % concentrations. NO conversion was determined in reduction by carbon monoxide in reaction mixtures containing 0.8 vol % NO and 0.9 vol % CO in a flow reactor at the gas flow rate 20000 h^{-1} on a monolith fragment 8 mm in diameter, 7 mm in height, and 0.18 g in weight.

For palladium-containing catalysts (0.1% Pd) with various concentrations of second supports, the temperature at which 50% CO conversion is reached served as a measure of catalytic activity. Application of up to 14.5% γ-Al_2O_3 (threefold impregnation) improves catalytic activities and increases specific surface areas to 16.5 m^2/g.

γ-Al_2O_3, %	0	6.3	10.2	14.5
Temperature of 50% CO conversion, °C	199	164	154	147

The catalyst where the second support is finely divided alumina is most active in three-way conversion reactions [37]. Table 3 displays the results of catalytic activity tests on a (0.18% Pt + 0.075% Pd + 0.026% Rh)/(Al_2O_3 + La_2O_3, CeO_2)/cordierite) catalyst sample.

Rare-earth oxides are known to be useful for controlling properties of low-percentage catalysts based on platinum-group metals. The effect of REOs on the properties of platinum in deep alkane oxidation catalysts has been studied most comprehensively [38]. When a platinum/alumina catalyst is doped with cerium oxide, platinum is stabilized in an oxidized state, probably, in the form of $PtO_xMe_nO_m$ [39]. As a result of the interaction between lanthanum oxide and palladium in Pd–La_2O_3/Al_2O_3 catalysts, these catalysts retain high activity in three-way conversion reactions even after treatment at 1000°C, in spite of a slight decrease in S_{sp} [40].

Table 3. Results of testing of the (Pt + Pd + Rh)/[Al_2O_3 + (La_2O_3, CeO_2)]/cordierite catalysts in three-way conversion reactions (gas flow rate: 20000 h^{-1})

Reaction	Temperature, °C, for conversion, %		
	50	80	90
CO + O_2 (1.6% CO in air)	225	232	235
n-C_6H_{14} + O_2 (1.1% n-C_6H_{14} in air)	252	282	310
NO + CO (0.8% NO, 0.9% CO in He)	347	352	355

Table 4. XPS data for Pd/Al_2O_3 (La_2O_3, CeO_2)/cordierite catalysts

Sample no.	REO percentage, wt %		Treatment temperature, °C	Electron binding energy, eV, for electronic states of elements			
	CeO_2	La_2O_3		Pd $3d_{5/2}$	O 1*s*	Si 2*p*	Al 2*p*
1*	0	0	550	337.0	532.2	102.4	74.5
2	0	0	550	335.3	531.9	102.6	74.2
3	0	0.15	550	336.1	531.9	102.6	74.1
4	0	0.15	850	335.8	531.9	102.5	74.0
5	0.15	0	550	335.0	532.1	102.7	74.1
6	0.15	0	850	335.0	531.8	102.4	74.0

* Sample 1 was examined as prepared; samples 2–6 after catalysis.

The thermal activation of a lanthanum oxide-modified palladium/alumina catalyst was described in [41]. This effect was manifested as an increase in the specific catalytic activity in the high-temperature reduction of nitrogen oxides by hydrocarbons after the catalyst was treated at 850°C. X-ray photoelectron spectroscopy (XPS) showed that this thermal activation is due to palladium stabilization in the form of Pd^{1+}.

Table 4 displays XPS data for $Pd/(Al_2O_3 + La_2O_3, CeO_2)$/cordierite catalysts. X-ray photoelectron spectra were recorded on a Kratos Analytical Series 800 XPS spectrometer using MgK_α radiation (1253.6 eV).

In a freshly prepared palladium/alumina catalyst (sample 1), palladium is in oxidized form; its valence state corresponds to Pd^{4+} (PdO_2) [42]. After the sample is treated by the reaction gas mixture at catalysis temperatures (sample 2), palladium acquires a near-metallic state and the $3d_{5/2}$ electron binding energy differs by 0.3 eV from the binding energy in metallic palladium (335.0 eV). Such a difference can result from agglomeration of metallic palladium. This suggestion agrees with the higher atomic catalytic activity of Pd^0 compared to Pd^{n+} [43].

The binding energy of palladium $3d_{5/2}$ electrons in the lanthanum oxide-modified catalyst (sample 3) corresponds to the oxidation state 2+ (PdO) [42]. In lanthanum oxide-modified sample 4, Pd^{1+} can appear after calcining at 850°C. This follows from the XPS spectrum, which is a well-defined doublet of the $3d_{5/2}$ and $3d_{3/2}$ electron states of palladium, and agrees with Shyu et al. [43], who considered the possibility of complex formation of cerium oxide with palladium where palladium is stabilized in the univalent state as $Pd^+O_2^-$ groups. In samples 5 and 6, most palladium occurs as the metal (Pd^0).

The above assignment explains the observed thermal activation of the lanthanum-containing catalyst and the absence of this effect for the CeO_2-modified catalyst, where palladium more readily transforms to the metallic state because of the low redox potential of cerium oxide (Table 4). Evidently, palladium stabilization in the form of Pd^{1+} increases the degree of dispersion of the active component, whereas metallic palladium can agglomerate. Although the atomic catalytic activity of Pd^{n+} can be lower than the activity of Pd^0, the specific catalytic activity of the catalyst increases, by analogy with platinum catalysts [44], because the active site concentration increases as a result of the increasing dispersion of the active component [45].

Thus, REOs in catalysts are multipurpose modifiers, improving the thermal stability of the second support and active phase and increasing the specific activity of platinum-group metals.

OXIDATION OF FINELY DIVIDED CARBON ON STRUCTURED OXIDE CATALYSTS

The combination of a soot filter and a soot oxidizer in one unit is the optimal solution for purifying diesel emissions from carbon particulates.

The results of design of catalytic coatings for soot filters based on transition-metal (Co, Mn, Cu, and Cr) oxides are summarized in [46]. The soot filter designed had a honeycomb structure where end-closed cells were arranged in the staggered order; this structure ensured the filtration of emissions through the walls of the monolith (wall thickness: 1.0 mm; cell size: 2.5 × 2.5 mm; open porosity: 43–48%; dominant pore size: 1–3 μm) [47].

The activity of binary oxide systems is noticeably higher than that of individual oxides: complete CO oxidation on cobalt oxide was reached at 197°C; on copper chromite and copper cobaltite samples, at 148 and 157°C, respectively. In the decreasing order of activities expressed as temperatures of 80% CO conversion, the catalysts are arranged as follows:

$$Co_3O_4 > MnO_2 > CuO > Cr_2O_3,$$

$$CuCr_2O_4 > CuCo_3O_5 > Co_3MnO_6 > CuMnO_3.$$

The temperature ranges of deep oxidation of *n*-hexane over individual and binary oxide catalysts are

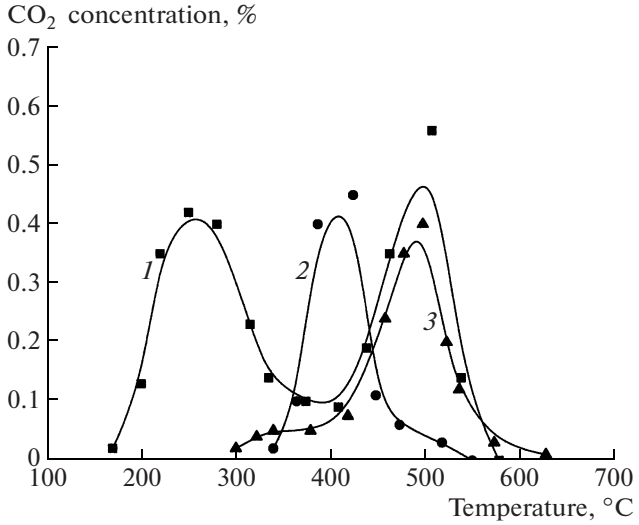

Fig. 3. CO_2 concentration versus the temperature of soot conversion by oxygen on (*1*) ($CuCr_2O_4 + Al_2O_3$)/cordierite, (*2*) K,Co/La_2O_3 [19], and (*3*) V_2O_5/MCM-41 [23].

differentiated not so strongly as for CO oxidation. In the decreasing order of activities expressed as temperatures of 80% *n*-hexane conversion, the catalysts are arranged as follows:

$$CuCr_2O_4 > CuCo_3O_5 > CuMnO_3 > Co_3MnO_6.$$

Comparison of the activity orders of the binary catalysts for CO and n-C_6H_{14} oxidations shows their similarity; copper chromite and copper cobaltite have higher activities.

The role of second supports having acidic surface properties (γ-Al_2O_3) for transition-metal oxide catalysts is not as simple as for platinum-metal three-way catalytic converters. This arises from possible ion-exchange interactions between transition-metal cations of the impregnating solution and acid surface sites. These interactions can yield low-activity associations linked to oxygen atoms of the support crystal lattice, which is inactive in deep oxidation reactions [48]. Studies into the effect of second supports on the catalytic properties of transition-metal-oxide-based contacts showed that, as the γ-Al_2O_3 percentage in the $CuCo_3O_5$/cordierite catalyst increases to 13.3 wt %, the activity of this catalyst in carbon monoxide and *n*-hexane oxidation decreases monotonically; this is manifested as 30–45°C increases in the temperatures of CO and n-C_6H_{14} 50% conversion [46] and can result from the effect of the strong interactions of the active component with the support.

To study soot combustion, we prepared cordierite-supported catalysts: (7.4% $CuCr_2O_4$ + 7.8% Al_2O_3) (1), (12.1% $CuCo_2O_4$ + 9.22% Al_2O_3) (2), and 17.6% $CuCo_2O_4$ (3).

Soot was applied to catalysts in a special cell whose design ensured exposure of all samples to diesel emissions under identical conditions [46].

Soot combustion was studied by temperature-programmed surface reactions using a quartz-spring balance and chromatography of combustion products (CO and CO_2). A catalyst sample (1 g; 0.5–1.0 mm particle sizes) was heated in flowing argon at 115°C for 3–4 h to remove adsorbed carbon dioxide and water [19]. After this, the sample was heated in flowing air while temperature increased at 4 K/min within 100–600°C and relative weight loss and gaseous reaction products percentages were recorded. Isothermal soot combustion experiments were carried out to determine the complete catalyst regeneration temperatures.

Soot oxidation by atmospheric oxygen [46, 47] showed that the catalyst coatings in the form of transition-metal oxides depress the reaction temperature. While the onset temperatures of vigorous soot combustion on the intact cordierite are above 500°C, on samples bearing catalyst coatings, they are 180–200°C with near-100% CO_2 selectivity.

Comparison of samples with identical catalytic coatings, one being free of a second support, showed that the temperature ranges of combustion of surface compounds have close values and the soot capacity of the sample coated with a second support is far higher. The intact cordierite has a far lower soot capacity; intense combustion of soot-like compounds starts at temperatures above 500°C, where regeneration on catalyst-coated samples already comes to the end [46, 47]. Therefore, the γ-Al_2O_3 second support increases the soot capacity of the filter and improves the selectivity of soot combustion to CO_2.

Of the catalysts tested, sample 1 shows the highest activity in soot conversion by atmospheric oxygen. On the curve plotting gaseous product emission from the surface of this catalyst as a function of linearly increasing temperature (Fig. 3, curve *1*), there are two CO_2 emission peaks at 270 and 490°C. Possible reasons for the appearance of these two peaks are the occurrence of several types of surface compounds with differing reactivities (hydrocarbons and highly dispersed carbon), which are produced by the reaction between the products of incomplete combustion of motor fuel and the catalyst surface, and the inhomogeneous fractional composition of carbon in engine emissions, as noted in [1]. Figure 3 also displays the emission of gaseous products of soot combustion (CO + CO_2) from the catalyst surface as a function of temperature for catalytic converters based on K/Co/La_2O_3 low-melting-point eutectic mixtures [19] (curve *2*) and V_2O_5 and MoO_3 individual oxide systems [23] (curve *3*). Comparing the curves plotted in Fig. 3, we find that the copper chromite catalyst is almost competitive in soot oxidation activity with Ba/Co/MgO and K/Co/CeO_2 systems described in [19, 30] and considerably exceeds, both in activity and selectivity, individual (molybdenum, vanadium, iron, and copper) oxides supported on various supports (SiO_2, SnO_2, and ZrO_2) [23].

Thus, $CuCr_2O_4$ and $CuCo_2O_4$ are the most active in oxidation of CO, *n*-hexane, and finely divided carbon.

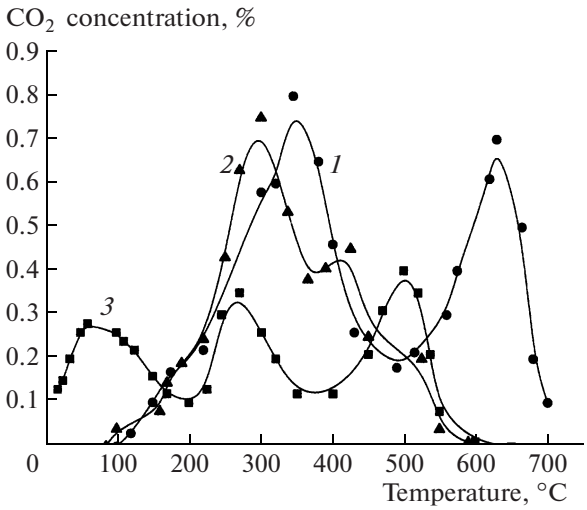

Fig. 4. CO_2 concentration versus the temperature of soot conversion in the presence of the ($CuCr_2O_4$ + Al_2O_3)/cordierite catalyst with various oxidizers: (*1*) NO, (*2*) NO_2, and (*3*) O_3.

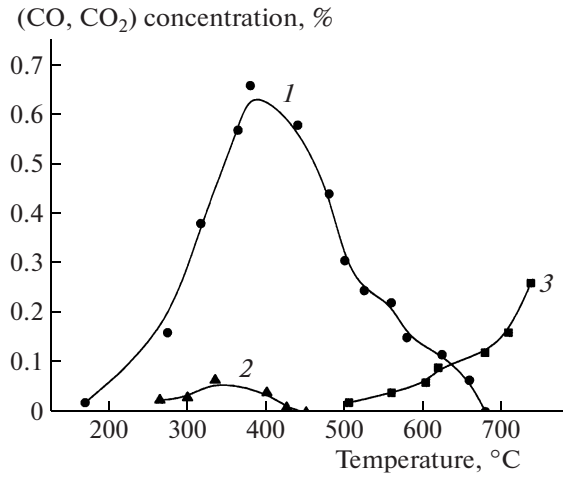

Fig. 5. (*1*) CO_2 and (*2*, *3*) CO emission concentration versus soot conversion temperature on the catalyst ($CuCo_2O_4$ + Al_2O_3)/cordierite with (*1*, *2*) H_2O and (*3*) CO_2 as oxidizers.

For reducing the regeneration temperatures of soot filters, the conversion of finely divided carbon was studied in the presence of various oxidizers contained in emissions from internal combustion engines (O_2, NO, NO_2, H_2O, O_2), as well as O_3, on soot filters coated with copper chromite or copper cobaltite catalyst coatings. Water and carbon dioxide are the main combustion products of motor fuels; their levels are far higher than for other oxidizers, and the water–gas shift reaction occurs at noticeable rates above 200°C [23]. Ozone in the presence of heterogeneous catalysts can recombinate to form highly reactive monooxygen. Ozone treatment is known to reduce the combustion temperature of diesel soot on $CuO–CeO_2–Al_2O_3$ catalysts on account of formation of stable oxygen radicals that react with carbon particulates [49, 50]. Therefore, the oxidation of diesel soot with ozone can occur at temperatures where other oxidizers are of low efficiency [51].

Figure 4 displays the temperature-programmed surface reaction curves to characterize CO_2 emission in soot conversion on the copper chromite catalyst (sample *1*) and the activities of various oxidizers in this reaction. From comparison of the curves plotted in Figs. 3 and 4, the onset temperatures of reactions involving NO and NO_2 (Fig. 4; curves *1*, *2*) are far lower than for the reactions involving O_2 (Fig. 3, curve *1*). Judging from the positions of the main CO_2 peaks, at higher temperatures soot burns out most vigorously in the presence of nitrogen(IV) oxide, whereas oxygen and nitrogen(II) oxide have far lower reactivities. The temperature at which soot completely burns out in the presence of NO_2 or O_2 is almost 100°C lower than in the presence of NO.

CO_2 was the only hydrocarbon product in these experiments, which implies that soot oxidation over the $CuCo_2O_4$ + Al_2O_3/cordierite catalyst involves the following reactions:

$$C + 2NO_2 \longrightarrow CO_2 + 2NO, \quad \text{(I)}$$

$$C + 2NO \longrightarrow CO_2 + N_2. \quad \text{(II)}$$

Ozone is the lowest temperature oxidizer. In the presence of the copper chromite catalyst (which is highly active in ozone decomposition), soot oxidation occurs with a higher intensity even at near-ambient temperatures, as indicated by the position of the first peak in the temperature-programmed surface reaction curve (Fig. 4, curve *3*). Above 190°C, finely divided carbon is oxidized by dioxygen (Fig. 3, curve *1*) and ozone (Fig. 4, curve *3*) within identical temperature windows because of high ozone decomposition rates under these conditions.

Inasmuch as CO_2 is also the only carbon-containing product in the experiments with ozone, the first stage of the reaction between carbon and ozone is ozone dissociation to highly reactive adsorbed monooxygen, which oxidizes carbon to CO, followed by its rapid oxidation to CO_2, and decomposes ozone to dioxygen:

$$\begin{gathered} O_3 + [\,] \longrightarrow O_2 + [O], \\ C + [O] \longrightarrow [CO], \\ [CO] + [O] \longrightarrow CO_2 + 2[\,], \\ O_3 + [O] \longrightarrow 2O_2 + [\,]. \end{gathered} \quad \text{(III)}$$

Soot oxidation by water vapor in the presence of the most active copper cobaltite catalyst (sample *2*) starts above 180°C (Fig. 5, curve *1*). The main carbonaceous product is CO_2; CO emission (curve *2*) is not high: noticeable carbon monoxide amounts are found only for the maximal reaction rate [52]. Evidently, soot

Table 5. Isothermal soot oxidation (gas flow rate: 100 ml/min)

Oxidizer	Carbon burnout, %, at temperature, °C							
	100	150	200	250	300	350	500	600
O_3 (0.14% in air)	60	84	98	100	100	100	100	100
NO_2 (5.0% in N_2)	0	0	31	71	94	100	100	100
H_2O (6.0% in N_2)	0	0	19	59	78	99	100	100
NO (5.0% in N_2)	0	0	15	54	72	98	100	100
O_2 (10.0% in N_2)	0	0	15	42	59	90	100	100
CO_2 (6.0% in N_2)	0	0	0	0	0	0	12	48

is oxidized by water vapor inside the diffusion layer by the reaction

$$C + 2H_2O \longleftrightarrow CO_2 + 2H_2, (\Delta H = +90.6\ \text{kJ/mol}) \quad \text{(IV)}$$

through the stages of carbon monoxide formation

$$C + H_2O \longleftrightarrow CO + H_2, (\Delta H = +132\ \text{kJ/mol}) \quad \text{(V)}$$

and subsequent conversion

$$CO + H_2O \longleftrightarrow CO_2 + H_2, (\Delta H = -41\ \text{kJ/mol}). \quad \text{(VI)}$$

The use of the γ-Al_2O_3 second support increases the catalyst activity [52], either because of the increasing dispersion of the active component (on account of the development of the pore structure) or because of stimulated water vapor adsorption (on account of increasing concentrations of Lewis acid surface sites) [26].

The interaction of soot with carbon dioxide by the reverse Boudoir reaction

$$C + CO_2 \longleftrightarrow 2CO\ (\Delta H = +172.5\ \text{kJ/mol}) \quad \text{(VII)}$$

becomes thermodynamically favorable at 430°C ($K_p = 0.8 \times 10^{-3}$), and in the presence of the copper chromite catalyst it occurs at noticeable rates above 500°C (Fig. 5, curve *3*).

For isothermal oxidation of soot (Table 5), the degree of catalyst regeneration at various temperatures can be quantified. Ozone provides high degrees of soot combustion at 100–150°C. In the presence of NO_2, NO, or O_2, soot combustion occurs at noticeable rates above 150°C. The reactivity of water vapor in conversion of finely divided carbon is higher than that of nitrogen(II) oxide or oxygen, indicating the utility of water vapor for catalytic oxidation of diesel soot. CO_2 has the lowest oxidation capacity toward diesel soot. Therefore, the reverse Boudoir reaction (VII) can hardly be considered as suitable for the regeneration of soot filters at the temperatures of engine emissions.

With respect to their reactivities in oxidation of finely divided carbon, the oxidizers tested are arranged in the following order:

$$O_3 \gg NO_2 > H_2O > NO > O_2 > CO_2.$$

The scenario of catalytic soot combustion was considered in [19, 23, 28]. The catalyst activity in the oxidation of finely divided carbon is frequently related to the "surface mobility" of the oxide coating. A certain combination of adsorption and oxidation–reduction properties of the catalyst surface ensures the adsorption and subsequent oxidation of soot. In this study, a second support (low-temperature Al_2O_3 phases) is used to control the adsorption properties of the catalyst for efficient soot adsorption and the use of oxidizers with elevated reactivities (NO_2, O_3, and H_2O) ensures the depression of the reaction temperature.

Engine bench tests on platinum-, palladium-, and ruthenium-containing catalysts supported on cordierite ceramic monolith matrices with γ-Al_2O_3 second supports modified by rare-earth oxides, showed high efficiency of these catalysts in the neutralization of CO, C_nH_m, and NO_x in diesel emissions even in the presence of excess oxygen concentrations; the designed soot filter provides a steady-state performance of the catalytic neutralizer [33].

The results of comparison tests carried out on AutoZAZ-Motor motor benches (AUTOZAZ-Daewoo, Melitopol) [53] showed that the designed catalytic converters are superior to state-of-the-art analogues produced by Walker (Germany) and Linda Gobex (Poland) (Fig. 6).

Studies of the effect of cerium, lanthanum, and other REO modifying dopants on the thermal stability of the pore structure of the second support (Al_2O_3 prepared by sol–gel technology) showed that the stabilizing effect of La_2O_3 is due to the formation of an La_2O_3 solid solution in Al_2O_3; this solid solution inhibits aluminum ion diffusion and retards the transition of low-temperature Al_2O_3 phases to high-temperature α-Al_2O_3. The thermal activation of the Pd/Al_2O_3/cordierite catalyst by lanthanum oxide was

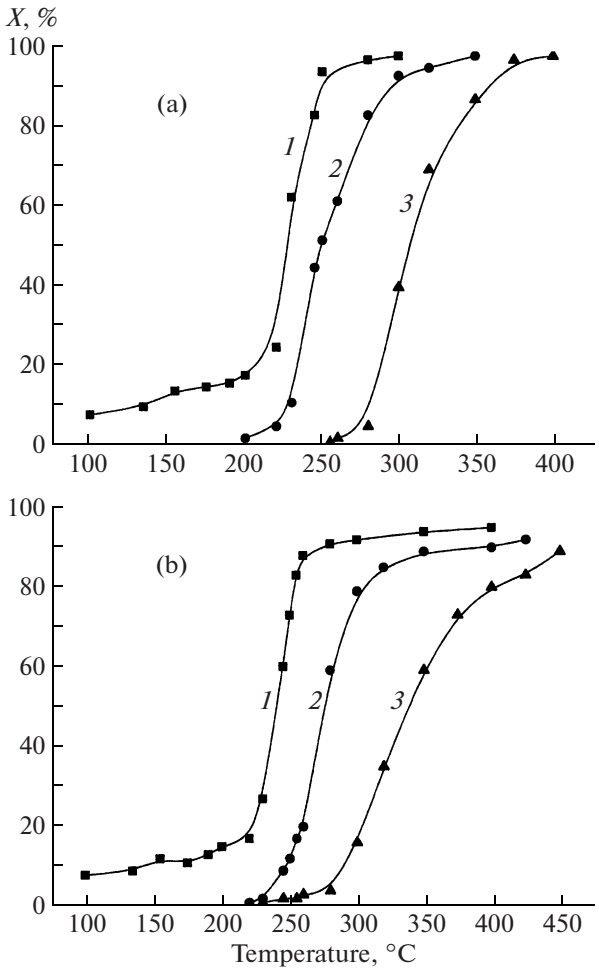

Fig. 6. Efficiency of catalysts in conversion of automobile emissions from (a) CO and (b) C_nH_m on an engine bench: (*1*) the newly developed catalyst, (*2*) Walker catalyst, and (*3*) Linda Gobex catalyst.

interpreted, proceeding from XPS data, as arising from the stabilization of singly charged palladium ($Pd^+O_2^-$) and the corresponding increase in the concentration of active sites.

Copper chromite is the most active catalyst coating of soot filters in CO and *n*-hexane oxidation reactions and in combustion of soot-like compounds. The use of binary oxide systems as catalytic coatings of soot filters and ozone as the oxidation initiator is helpful to approach the problem of low-temperature complex conversion of emissions, known as the "cold start" problem.

To summarize, efficient three-way conversion catalysts in combination with catalyst-coated soot filters constitute the basis for technology of the two-step conversion of emissions of internal combustion engines.

REFERENCES

1. Kaspar, J., Fornasiero, P., and Hickey, N., *Catal. Today*, 2003, vol. 77, no. 4, p. 419.
2. Farrauto, R.Dzh. and Khek, R.M., *Kinet. Katal.*, 1998, vol. 39, no. 5, p. 646 [*Kinet. Catal.* (Engl. Transl.), vol. 39, no. 5, p. 594].
3. Popova, N.M., *Katalizatory ochistki vykhlopnykh gazov avtotransporta* (Automobile Exhaust Neutralization Catalysts), Alma-Ata: Nauka, 1987.
4. Walker, A.P., *EuropaCat V, Book 3 of Abstracts*, Limerick, Ireland, 2001, p. 7-01.
5. Fornasiero, P., Di Monte, R., Ranga, RaoG., and Kaspar, J., *J. Catal.*, 1995, vol. 151, no. 1, p. 168.
6. Vlaic, G., Fornasiero, P., Geremia, S., and Kaspar, J., *J. Catal.*, 1997, vol. 168, no. 2, p. 386.
7. Ivanova, A.S., Moroz, E.M., and Polyakova, G.A., *Kinet. Katal.*, 1994, vol. 35, no. 5, p. 786.
8. Piras, A., Trovarelli, A., and Dolcetti, G., *Appl. Catal., B*, 2000, vol. 28, no. 2, p. L77.
9. Koryabkina, N.A., Shkryabina, R.A., Ushakov, V.A., et al., *Kinet. Katal.*, 1996, vol. 37, no. 1, p. 117 [*Kinet. Catal.* (Engl. Transl.), vol. 37, no. 1, p. 117].
10. Morterra, C., Magnacca, G., Bolis, V., Cerrato, G., et al., in *Catalysis and Automotive Pollution Control*, Frennet, A. and Bastin, J.M., Eds., Amsterdam: Elsevier, 1995, vol. 3, p. 361.
11. Heck, R.M. and Farrauto, R.J., *Catalytic Air Pollution Control: Commercial Technology*, New York: Van Nostrand Reinhold, 1995, p. 1.
12. Matsumoto, S., *Catal. Today*, 2004, vol. 90, nos. 3–4, p. 183.
13. Haruta, M. and Date, M., *Appl. Catal., A*, 2001, vol. 222, nos. 1–2, p. 427.
14. Centi, G., Arena, G.E., and Perathoner, S., *J. Catal.*, 2003, vol. 216, nos. 1–4, p. 443.
15. Zav'yalova, U.F., Tret'yakov, V.F., Burdeinaya, T.N., et al., *Khim. Interes. Ust. Razv.,* 2005, vol. 13, p. 751.
16. Gandhi, H.S., Graham, G.W., and McCabe, R.W., *J. Catal.*, 2003, vol. 216, nos. 1–2, p. 433.
17. Heck, R.M. and Farrauto, R.J., *Appl. Catal., A*, 2001, vol. 221, nos. 1–2, p. 443.
18. Webster, D.E., *Top. Catal.*, 2001, vols. 16–17, nos. 1–4, pp. 33–38.
19. Pisarello, M.L., Milt, V., Peralta, M.A., et al., *Catal. Today*, 2002, vol. 75, nos. 1–4, p. 465.
20. Van Setten, B.A.A.L., Scouten, J.M., Makee, M., et al., *Appl. Catal., B*, 2000, vol. 28, nos. 3–4, p. 253.
21. Jelles, S.J., Krul, R.R., and Makkee, M., *Catal. Today*, 1999, vol. 53, no. 4, p. 623.
22. Jelles, S.J., Makkee, M., Moulijn, J.A., et al., *SAE Paper 990113*, 1999.
23. Liu, S., Obuchi, A., Uchisawa, J., et al., *Appl. Catal., B*, 2000, vol. 37, no. 4, p. 309.
24. Van Setten, B.A.A.L., Makee, M., and Moulijn, J.A., *EuropaCat V, Book 3 of Abstracts*, Limerick, Ireland, 2001, p. 7-19.
25. Van Setten, B.A.A.L., Van Dijk, R., and Jelles, S.J., *Appl. Catal., B*, 1999, vol. 21, no. 1, p. 51.

26. Saracco, G., Badini, C., Russo, N., and Specchia, V., *Appl. Catal., B,* 1999, vol. 21, no. 4, p. 233.
27. Ciambelli, P., Palma, V., Russo, P., et al., *Catal. Today*, 2002, vol. 75, nos. 1–4, p. 471.
28. Miro, E.E., Ravelli, F., Ulla, M.A., et al., *Stud. Surf. Sci. Catal.*, 2000, vol. 130, p. 731.
29. Makkee, M., Krijnsen, H.C., Bertin, S.S., et al., *Catal. Today*, 2002, vol. 75, nos. 1–4, p. 459.
30. Obuchi, A., Oi-Uchisawa, J., Enomoto, R., et al., *Stud. Surf. Sci. Catal.*, 2000, vol. 130, p. 1559.
31. Ismatov, Kh.R. and Abdullaev, A.B., *Zh. Prikl. Khim.*, 1970, vol. 43, no. 3, p. 668.
32. Dzis'ko, V.A., *Kinet. Katal.*, 1979, vol. 20, no. 6, p. 1526.
33. Solov'ev, S.A., Beiman, A., Pavlikov, V.N., et al., *Katal. Neftekhim.*, 2003, no. 11, p. 63.
34. Shaper, H., Doesburg, E.B., and Van Reijen, L.L., *Appl. Catal., B*, 1983, vol. 7, no. 2, p. 211.
35. Vereshchagin, V.I., Zelinskii, V.Yu., Khabas, G.A., and Kolova, I.I., *Zh. Prikl. Khim.*, 1982, vol. 55, no. 9, p. 1946.
36. Mokhnachuk, O.V., Solov'ev, S.A., Il'in, V.G., et al., *Teor. Eksp. Khim.*, 2006, vol. 42, no. 5, p. 318.
37. Solov'ev, S.A., Kurilets, Ya.P., and Orlik, S.N., *Teor. Eksp. Khim.*, 2003, vol. 39, no. 1, p. 50.
38. Drozdov, V.A., Tsyrul'nikov, P.G., Popovskii, V.V., et al., *Kinet. Katal.*, 1986, vol. 27, no. 1, p. 162.
39. Chzhu, D.P., Tsyrul'nikov, P.G., Kudrya, E.N, et al., *Kinet. Katal.*, 2002, vol. 43, no. 3, p. 410 [*Kinet. Catal.* (Engl. Transl.), vol. 43, no. 3, p. 379].
40. Kim, D.H., Woo, S.I., and Lee, J.M., *Catal. Lett.*, 2000, vol. 70, nos. 1–2, p. 35.
41. Mokhnachuk, O.V., Solov'ev, S.A., and Senkevich, A.I., *Teor. Eksp. Khim.*, 2006, vol. 42, no. 1, p. 44.
42. Kim, K.S., Grossmann, A.F., and Winograd, N., *Anal. Chem.*, 1974, vol. 46, no. 2, p. 197.
43. Shyu, J.Z., Otto, K., Watkins, W.L.H., et al., *J. Catal.*, 1988, vol. 114, no. 1, p. 23.
44. Burch, R., Crittle, D.J., and Hayes, M.J., *Catal. Today*, 1999, vol. 47, nos. 1–4, p. 229.
45. Mokhnachuk, O.V., Soloviev, S.O., and Kapran, A.Yu., *Catal. Today*, 2007, vol. 119, nos. 1–4, p. 145.
46. Solov'ev, S.A., Kurilets, Ya.P., Orlik, S.N., Pavlikov, V.N., and Garmash, E.P., *Teor. Eksp. Khim.*, 2003, vol. 39, no. 5, p. 317.
47. Solov'ev, S.A and Orlik, S.N., *Katal. Prom–sti.*, 2007, no. 5, p. 23.
48. Tagiev, D.B. and Minachev, Kh.M., *Usp. Khim.*, 1981, vol. 50, no. 11, p. 1929.
49. Bokova, M.N., Pryakhin, A.N., Lunin, V.V., Dekarn, K., et al., *Katal. Prom–sti.*, 2003, no. 6, p. 36.
50. Bokova, M., Decarne, C., Abi-Aad, E., et al., *Appl.Catal., B*, 2004, vol. 54, p. 7.
51. Gomez-Serrano, V., Alvarez, P.M., Jaramillo, J., and Beltran, F.J., *Carbon*, 2002, vol. 40, no. 4, p. 513.
52. Solov'ev, S.A., Kurilets, Ya.P., and Orlik, S.N., *Teor. Eksp. Khim.*, 2005, vol. 41, no. 5, p. 307.
53. Soloviov, S.O. and Orlik, S.M., *Nauka Innov.*, 2005, vol. 1, no. 2, p. 58.